CONTRIBUTIONS TO THE INTOR WORKSHOP

UCID--21279

DE88 004149

July 1987

Compiled by J. R. Miller

1. Higher current densities in TF coils with Nb_3Sn conductors are not disallowed, but their achievement depends more or less on developments in several areas: protection schemes and insulation systems that allow coils to be dumped safely with high terminal voltages (of the order of 20 kV), conductors with higher current capacity (25 kA or greater) and suitable formability, and wind-and-react techniques to minimize the degradation of the current-carrying capacity of the Nb_3Sn conductors. These areas will be re-examined and the data base surveyed before the next session. The results will also be useful for assessing manufacturability and attainable current densities in the PF coils.

The state of the art for magnets using Nb_3Sn has not changed significantly since the December INTOR Workshop. Our conclusions about higher attainable TF coil current densities presented at the December workshop also remain essentially unchanged. To reiterate, we attain high TF winding pack current densities by an integrated design approach whereby we attempt to preclude any single factor from limiting the design more than others.

We begin by keeping the machine size as small as possible by minimizing the thickness of nuclear shielding. Nb_3Sn has a high, usable, temperature margin, even at high fields and current densities, which allows the acceptance of high nuclear heat loads in the winding pack. Compactness of the magnet system greatly alleviates structural and quench protection problems and significantly relaxes the constraints on current density. We further alleviate the protection problem by choosing high operating current (36 kA in the TIBER-II design) and, coincidentally, improve heat removal capabilities as well by shortening the flow paths. Both effects allow further gains in overall current density. Although conductor current is high, the conductor size is not unmanageable because the current density has been kept high.

We also use a cable-in-conduit conductor system in which the components have been well optimized for high performance under the operating conditions, taking full account of the conduit as distributed structure for partial support of the TF system bursting loads, with a realistic assessment of the strain condition of the Nb_3Sn composite conductor strands, and with an accounting for radiation damage to the conductor stabilizer during the operating life of the machine. TF coil winding-pack parameters obtained in the TIBER-II design process are given in Table 1.

Although our TF conductor is reasonably small in the bend direction, we propose winding and then reacting individual pancakes of the TF coils to attain maximum performance from the Nb_3Sn. The pancakes can be individually insulated with radiation tolerant insulating materials after the reaction heat treatment, then assembled into a case and potted. This is exactly the method of fabrication used for the MIT 12-T coil module. We envisage similar design and fabrication approaches for the PF system coils. For the

TABLE 1. TF COIL WINDING PACK PARAMETERS

NI = 5.2 MA/coil	Overall winding pack, materials fractions
A_{pack} = 0.130 m^2	f'_{steel} = 0.37
J_{pack} = 40 A/mm^2	f'_{insul} = 0.06
I_{op} = 36 kA	f'_{cond} = 0.34
A_{eff} = 904 mm^2 (26.9 mm × 33.6 mm)	f'_{He} = 0.23
	Cable fractions
A_{cs} = 514 mm^2	f_{cond} = 0.6 (fraction of conductor in cable space)
J_{cs} = 70 A/mm^2	f_{Cu} = 0.6 (fraction of copper in conductor)
	Cable pattern
	5 × 5 × 5 × 3 × 1.02 mm dia.

central solenoid modules, we have produced feasible designs with similar winding-pack current density to the TF coils, but with higher maximum fields possible because of the absence of nuclear heating in these coils.

2. The fault condition in the event that the quench protection system does not work will be analyzed. In such a situation, the protection of the coil against damage is secondary. Rather, the safety of personnel and the prevention of a catastrophic failure of the facility is the goal. This may or may not impose a more severe limit on current density than other constraints.

The analysis of the outcome of a fault condition wherein the quench protection of a TF system fails to operate will be extremely complex. For our design, if the analysis is to be reliable, it must be supported by data on quench propagation in cable-in-conduit conductors. These data are extremely limited at present. We feel such analysis is greatly needed, but should be postponed until the required data base is accumulated.

3. The temperature margin provided by forced-flow cooling of NbTi conductors with He II will be reassessed and an evaluation made of the risks of this technique relative to forced-flow cooling of Nb_3Sn conductors at 4.5 K.

The temperature margin provided in a TF system using NbTi conductors and forced-flow cooling with He II is small, even when the nuclear shield is very thick. Operation at He-II temperatures will increase refrigeration operating costs by nearly a factor of 3 over a 4.5 K system handling the same heat load. Capital costs will be higher by a similar factor. With the temperature margins available from a Nb_3Sn-based TF system, much higher heat loads can be tolerated. Studies using detailed helium properties and realistic nuclear heating scenarios have shown quite high temperature margins retained in the TIBER-II TF system with total heat loads of greater than 70 kW, even with 12 T maximum field and 40 A/mm² winding pack current density (cf. Fig. 1). By comparison, a very clever NbTi/He-II design offered by the European team showed rapidly diminishing margins at about 11 T and just over 20 A/mm² winding-pack current density.

4. A comparison of the overall current density available using the "Wedging" or "Bucking" approach for the TF coils will be made.

This comparison has not been carried out for superconducting coils, but a study of the trade-offs for wedging, bucking, and a combination of the two (if somehow that could be achieved) has been performed by the group at MIT/PFC. A copy of that study is attached as an appendix.

5. The allowable stresses in the structural material are affected by many factors:

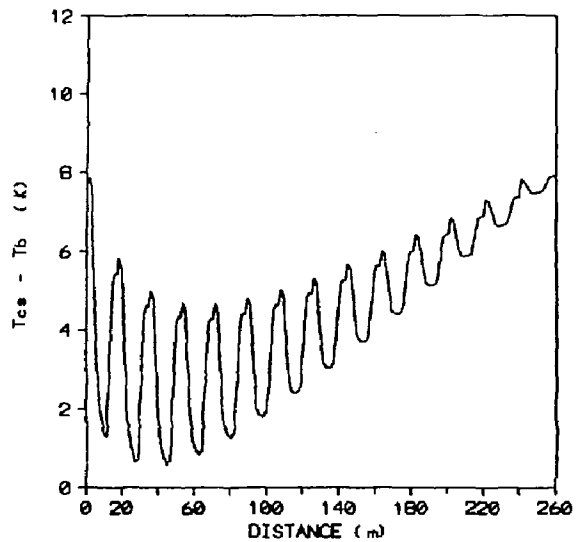

72 kW

Fig. 1. Temperature margin in a TIBER-II TF coil with high nuclear heat load.

a. Loading conditions (e.g. static, cyclic),
b. Material status (e.g. thermomechanical pretreatment),
c. Type of alloy,
d. Definition of stresses (e.g. primary, secondary).

Each delegation shall define the level of allowable stresses in their design, specifying under which of the above mentioned conditions the stress limit is applicable.

The structural materials in the the TIBER-II design can be divided into two broad classes: magnet case and distributed structure (superconductor conduit). The allowable stresses in these materials are determined by loading conditions (static, cyclic), thermomechanical treatment, alloy composition, and stress definition.

The stress allowables for both the case materials and distributed structure are determined by placing a limit on the Von Mises' combined stress. Combined stresses are limited to the lower of two-thirds yield stress or one-half ultimate strength. Membrane and bending stresses are limited to two-thirds yield and nine-tenths of yield strength, respectively.

The materials selected for the magnet case are 304 LN and 316 LN. The liquid-helium-temperature yield strengths of 316 LN are slightly higher than 304 LN, making it useful in components where operating stresses are high. Wherever possible, 304 LN is preferred due to its ready availability in thick sections. The distributed structural material of the PF and TF coils will be JBK-75 (an A-286 variant) or Incoloy 9XA. Both alloys are precipitation-hardening steels with thermomechanical treatments that are compatible with Nb_3Sn processing. JBK-75 is a stainless, austenitic steel; Incoloy 9XA is a non-stainless, low thermal expansion, austenitic alloy. Incoloy 9XA will result in lower precompression of the conductor by thermal cooldown strains. However, it must always be remembered that part of the precompression may be offset by the tensile strains inherent during operation. Final alloy selection will depend on a detailed analysis of conductor strain sensitivity, prestrain, magnet design, operating forces, and operating strains.

Base- and weld-metal mechanical properties of the alloys under consideration are shown in Tables 2 and 3. The 4 K mechanical properties of 304 LN and 316 LN are for the annealed condition. The properties of JBK-75 and Incoloy 9XA are given for alloys which have been given a simulated Nb_3Sn reaction heat treatment. All alloys have an excellent combination of strength and toughness at low temperature.

The mechanical properties of 304 LN and 316 LN weldments are variable, being dependent upon the joining process and filler metal selected. Typical cryogenic mechanical properties of austenitic welds are shown in Fig. 2. We anticipate that welded construction can be used, provided weld stresses are minimized and appropriate welding procedures are utilized.

TABLE 2. BASE METAL MECHANICAL PROPERTIES (4.2 K)

Material	Yield (MPa)	Ultimate (MPa)	Fracture Toughness ($MPa\sqrt{m}$)
304 LN (annealed)	810	1700	255
316 LN (annealed)	980	1500	270
JBK-75 (aged)	1300	1790	100
Incoloy 9XA (aged)	1150	1780	110

TABLE 3. WELD METAL MECHANICAL PROPERTIES (4.2 K)

Material	Yield (MPa)	Ultimate (MPa)	Fracture Toughness (MPa$\sqrt{m}$)
304 LN (annealed)		Properties are highly variable, depending on process and filler metal selected (see attached).	
316 LN (annealed)			
JBK-75 (aged) (autogenous GTAW)	1330	1840	140
Incoloy 9XA (aged) (autogenous GTAW)	1190	1720	110

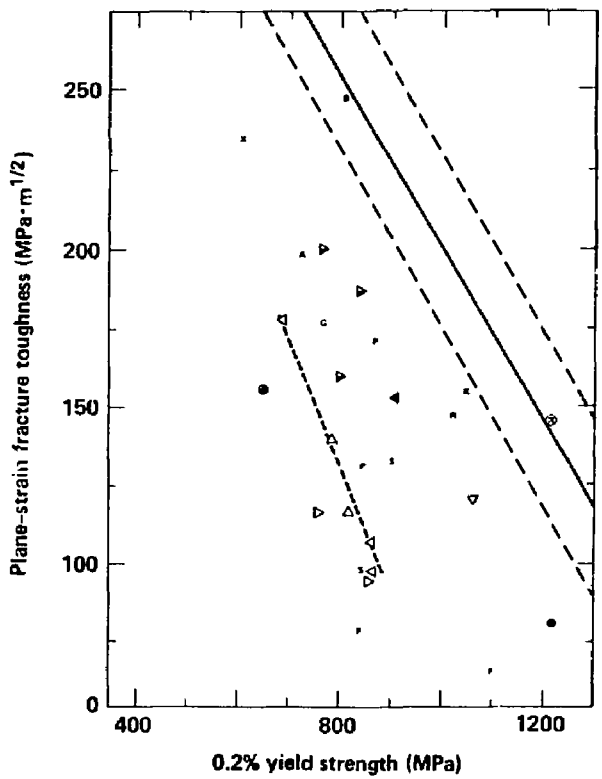

Symbol	Filler metal	Base metal	Process
B	FOX TT-250	316L	SMA
▷	316L-15	316LN	SMA
▶	316L-15	304LN	SMA
P	316L-15	316LN	SMA [a]
A	316L-15	316LN	SMA [b]
◁	316L-16	304L	SMA
◀	316-16	304L	SMA
⊕	308L-15	316LN	SMA
F	308L	304L	FCMA
G	308L	304L	GMA
S	316L	316LN	SA
X	16-16-2 Cr-Ni-Mo	304L	FCMA
▽	18-16-9 Cr-Ni-Mn	304L	GMA
K	KROMARC	58	GTA
●	NITRONIC	40	GTA
△	310-16	310S	SMA
R	20-16-6	20-16-6	SA
Ⓡ	Cr-Ni-Mn	Cr-Ni-Mn	GMA

[a] Weld peened after each pass

[b] As in above note, also 1311 K, 1 h, fan air cool after welding

Fig. 2. Cryogenic mechanical properties of welds in austenitic materials.

Finite-element-analysis (FEA) methods have been used to evaluate the maximum stresses in the TF coil magnet case. The stresses for the inner and outer legs are shown in Table 4. The operating stresses are below the specified allowables. Due to the simple geometry of the PF coils, the individual windings can be designed to be self supporting; therefore, no significant loads are carried by the external magnet case.

Analysis of the stresses in the distributed structure of the TF coils has also been carried out. The maximum of the mean von Mises' combined stress due to tension, centering, and overturning is 470 MPa, well below allowable limits. An example of the conduit and the distributed structure design appears in Fig. 3 with a notation of the mean principal stresses and the von Mises combinations of these.

Hoop strains in the PF central solenoids are a function of coil position and operating mode. In TIBER II, the TF coils butt directly against the central solenoid of the PF system. When the TF coils are energized, the central solenoid modules are effectively put in compression. If they are simultaneously energized, their electromagnetic forces tend to offset the compression imposed by the TF coil set. A plot of hoop strain vs radial position in the windings of coil modules 11 and 12 (middle of the central stack) is shown in Fig. 4. Strains would be highest if the PF coils were energized alone and unsupported by the TF coils (von Mises' stress = 555 MPa).

Cyclic operation of the PF system will be required for inductive operation, which will introduce cyclic loads in the distributed coil structure. The stress cycles would be tensile and at a maximum if the central solenoid were unsupported by the TF coils. The combined von Mises' stress would be approximately 555 MPa in the highest-stress region of these coils. If the central solenoid is supported by the TF system, the windings remain slightly in compression at the peak operating current.

Excellent cryogenic fatigue-crack-growth data for JBK-75 is available as a result of the Westinghouse LCT program. Using this data and the calculated stresses, we can approximate the fatigue life of unsupported central solenoid coils. For calculation, we have assumed a sheath wall thickness of 2.3 mm and a flaw detection limit of 10% (0.23 mm). We have furthermore assumed that the coils are cycled from full to zero field during operation. For the case of a 2.3-mm-thick sheath, we have plotted the number of cycles to failure N vs alternating stress $\Delta\sigma$, as shown in Fig. 5. For an alternating stress of 555 MPa, the number of cycles to failure is approximately 40,000. If we assume a safety factor of 4:1, the useful coil life is reduced to approximately 10,000 cycles. The problem of fatigue in the central solenoid will be greatly alleviated by supporting them against the TF system, since the windings remain in compression throughout each cycle.

TABLE 4. STRESSES - TF COIL CASE (316 LN)

Position	Bending (MPa)	Membrane (MPa)	Shear (MPa)	Combined (MPa)
Outer leg	630	93	---	630
Inner leg	---	265	410	488

Maximum allowable two-thirds yield = 653 MPa

One-half ultimate = 750 MPa

$\sigma_T \approx$ **250 MPa**

$\sigma_R \approx$ **410 MPa**

$\sigma_X \approx$ **280 MPa**

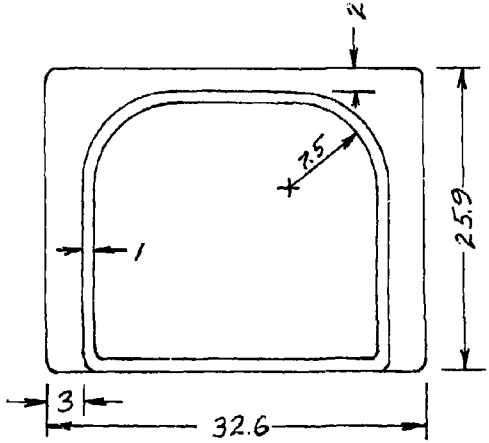

$\sigma_{VME} \approx$ **470 MPa in legs**

$\approx$ 380 MPa in web

Fig. 3. TIBER-II conductor structural channel.

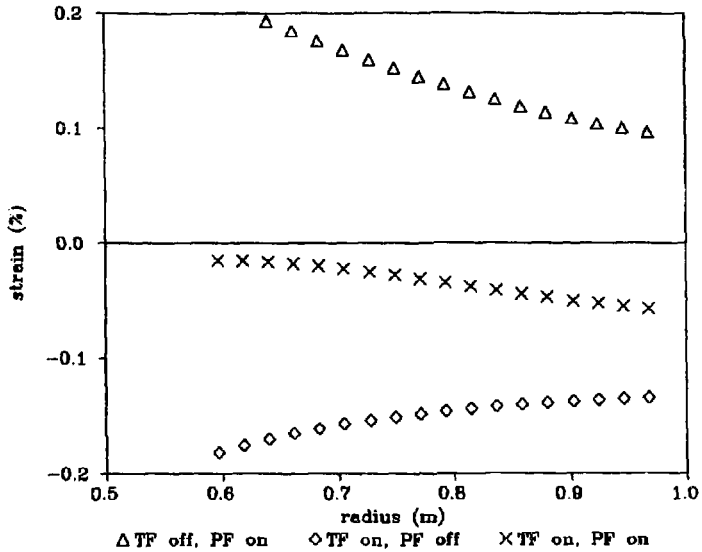

Fig. 4. Hoop strains in PF central solenoid modules 11 and 12 for the combinations of TF/PF energization.

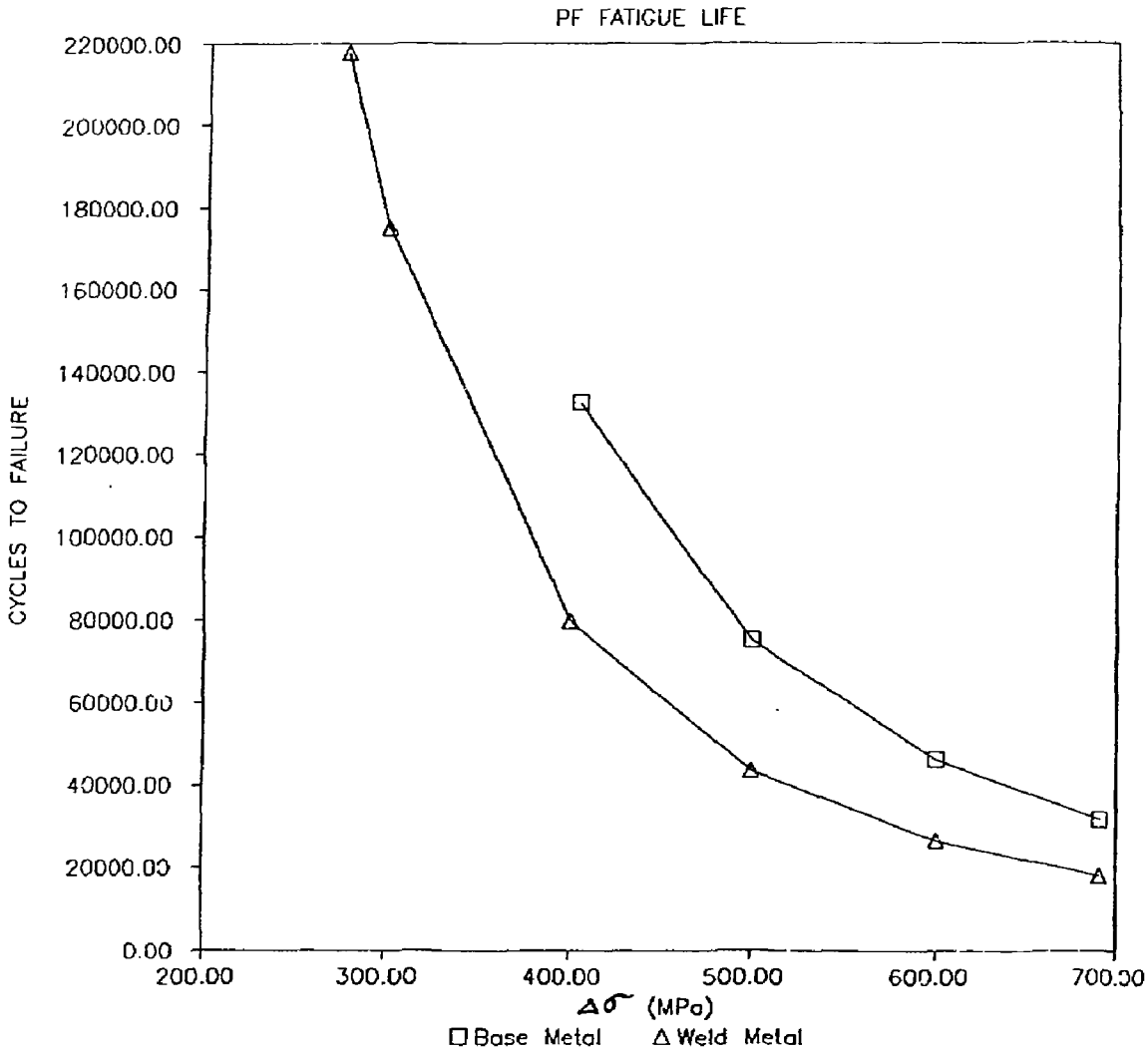

Fig. 5. Fatigue life in the TIBER-II central solenoid if the coils are unsupported by the TF system.

APPENDIX

BUCKING AND WEDGING CONSIDERATIONS FOR CIT*

D. B. Montgomery, J. Chen, H. Becker
Plasma Fusion Center
May 1987

1.0 INTRODUCTION

Tokamak designers have utilized various structural strategies to support the TF coils against the inward in-plane load arising from the toroidal field, and against the out-of-plane twists arising from the interaction of the TF coils with the poloidal fields. Table 1 lists six machines representing a spectrum of approaches. Three machines utilize bucking, and three wedging, to support in-plane inward loads. Two of the bucked machines react the center region torque by keying the coil noses against a support structure and one (JT-60), reacts the torque only in the coil cases. The three wedged machines resist torque by shear in the wedged center leg. Three of the machines have internal PF coils, and three have external PF coils.

All the machines in Table 1, avoid combined bucking and wedging in the central leg regions by choosing assembly clearances to assure either pure bucking or pure wedging.

* Also see Addendum: "Heating Considerations", May 1987

TABLE 1
SUPPORT CONCEPTS USED IN REPRESENTATIVE TOKAMAKS

DEVICE	IN-PLANE SUPPORT	OUT-OF-PLANE SUPPORT	LOCATION OF PF COILS
TFTR	BUCKED	COIL CASE	EXTERNAL
JT-60	BUCKED	COIL CASE	INTERNAL
JET	BUCKED	TORQUE TUBE	EXTERNAL
DIII-D	WEDGED	COLUMN SHEAR	INTERNAL
ASDEX-U	WEDGED	COLUMN SHEAR	EXTERNAL
ALCATOR C-MOD	WEDGED	COLUMN SHEAR	INTERNAL

TABLE 1 NOTES

TFTR

TF cased coils bucked from rings interleaved with central OH; coil cases keyed to center post; shear panels wedged at OD; outer section torque through outer TF coil cases.

JT-60

TF cased coils bucked from rotatable disks on center post; external torque frame.

JET

TF coils uncased in central region; coil noses keyed into thin split torque tube which transfers in-plane bucking load to OH solenoid wound on center post; shear keys between TF coil turns; external torque shell.

DIII-D

TF turns bonded into monolithic cylinder; radial preload; external torque frame.

ASDEX-U

Prebonded coils wedged with small preload; external torque shell.

ALCATOR C-MOD

TF turns bonded into monolithic cylinder; external torque shell.

2.0 IDEAL BUCKING, WEDGING, AND COMBINED BUCKING WEDGING

It is useful to examine the relative structural efficiency of bucking, wedging, and combined bucking and wedging in an ideal case.[1] By "ideal" is meant no allowance for assembly clearances, temperature differences, or variations in modulus. We can illustrate the relative efficiency by using the simple cylindrical representation of the TF central region shown in Figure 1. We will neglect the axial tension from the vertical load on the top and bottom of the TF coil (ie, we will assume it is cancelled by axial preload) and will neglect any reduction in wedge pressure due to outward loads on the outer legs. A set of equations can then be derived for stresses resulting from a uniform distribution of current in the cylinder (Appendix A), and the results given in Figures 2-4. Figure 5 then plots the peak stresss from Figures 2-4.

Figure 2 shows the distribution of principal stresses for a simple wedged design, for two cylinders of different α (outer to inner radius ratio). In the cases considered, the radial stress and coil face pressure (hoop stress) are both compression. Consequently, the tresca stress, (defined as equal to the maximum difference of principal stresses) is equal to the face pressure minus the vertical stress, (here assumed zero) and consequently is equal to the face pressure stress alone. The stresses are normalized to $(B_c^2/2\ \mu_o)$, where B_c is the resultant field at the surface of the cylinder. For example, using Figure 2B, a magnet with $\alpha = 3$, has a normalized

peak stress of 3.2 and hence at B_c = 10 T, has a tresca stress of $(10^2/0.8\ \pi)$ x 3.2 = 127 MPa.

Figure 3 shows the distribution of principal stresses for two bucked cylinders of different α. Unlike the wedged case, where both radial and face compression were present, now only the radial stress is present, and is a maximum at the interface with the bucking post.

Figure 4 shows the distribution of principal stresses for an ideal combined bucking and wedging case, again for two radius ratios. As in the wedged case, the combined tresca stress, is equal to the face pressure.

Figure 5 plots the peak tresca stress for each of the three above cases, as a function of the ratio α. Several important general conclusions can be drawn from this figure:

(i) Ideal combined bucking and wedging results in lower peak stresses than either alone, for all radius ratios.

(ii) Ideal bucking and wedging being somewhat "hydrostatic" in nature, is only weakly dependent on the radius ratio.

(iii) At large radius ratios pure wedging results in a peak stress twice that of combined bucking and wedging. Intuition might have led one to expect them to be equal in this limit, but the wedged case always has a "hole", which no matter how small, results in a stress concentration factor of two.

(iv) Below a radius ratio of 2.6 pure bucking shows lower stresses than pure wedging, and approaches the same peak stress as combined bucking and wedging, as the radius ratio is reduced toward 1.0.

Figure 6 adds to Figure 5, the average wedging stress in the pure wedging case. The average wedging stress is of interest to the designer, because in pure wedging, the average hoop stress is the membrane stress (usually compared with 2/3 of yield to evaluate survivability). In pure bucking, the primary membrane stress must be taken as the peak stress.

We note from Figure 6, that the average wedging stress approaches the combined bucking and wedging stress in the limit of a thick cylinder; the average stress averages out the stress concentration of the central hole. Above a radius ratio of 2, the average wedging stress is less than the peak bucking stress. Magnets compared on a membrane stress basis would therefore favor wedging for α greater than 2.

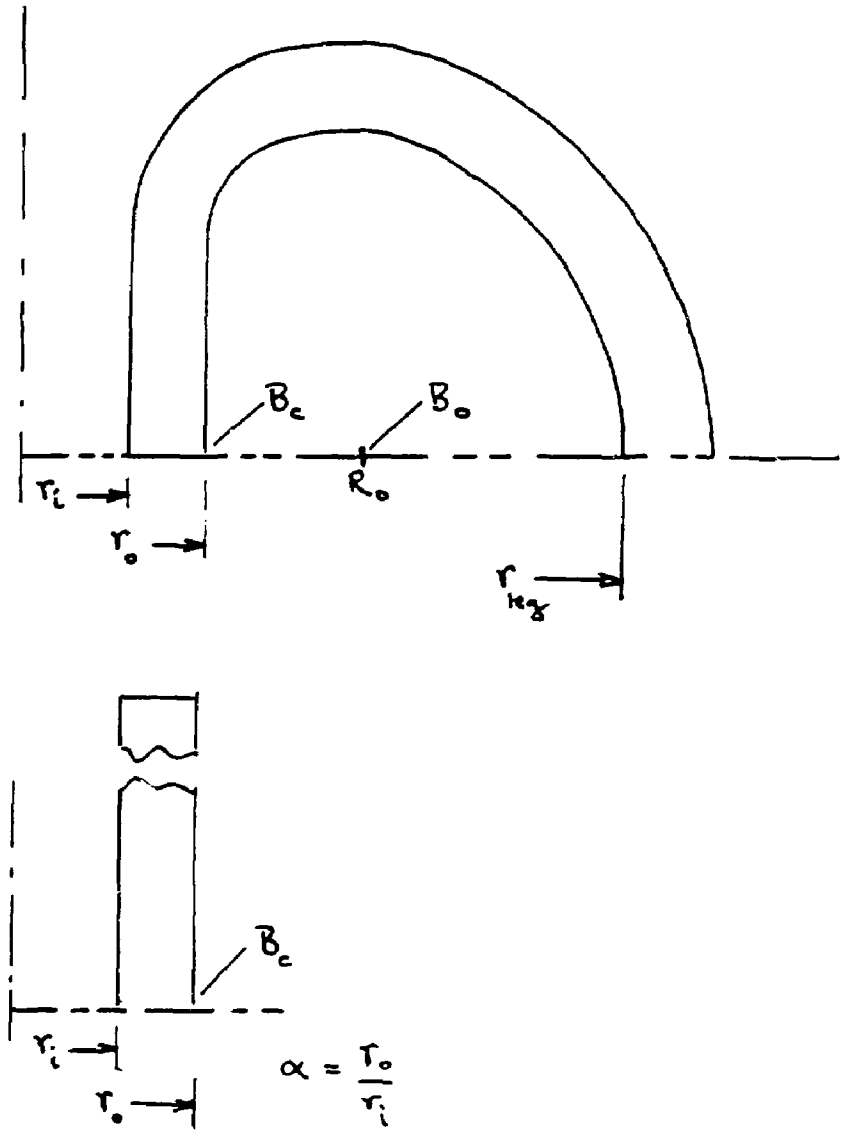

Figure 1: Idealized toroidal shell, and cylindrical approximation of central region.

2A DISTRIBUTION OF PRINCIPAL STRESSES ACROSS THE THICKNESS IN PURE WEDGING

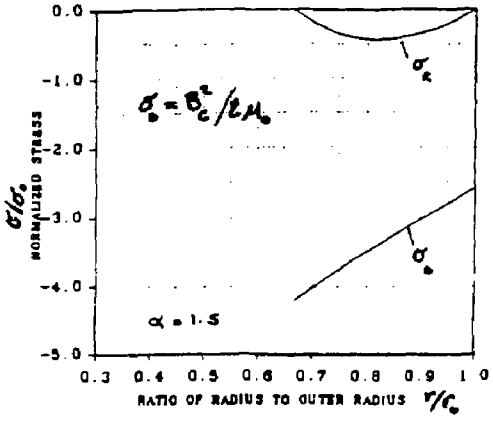

2B DISTRIBUTION OF PRINCIPAL STRESSES ACROSS THE THICKNESS IN PURE WEDGING

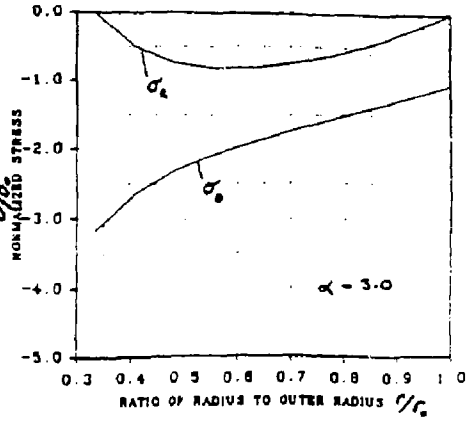

3A DISTRIBUTION OF PRINCIPAL STRESS ACROSS THE THICKNESS IN PURE BUCKING

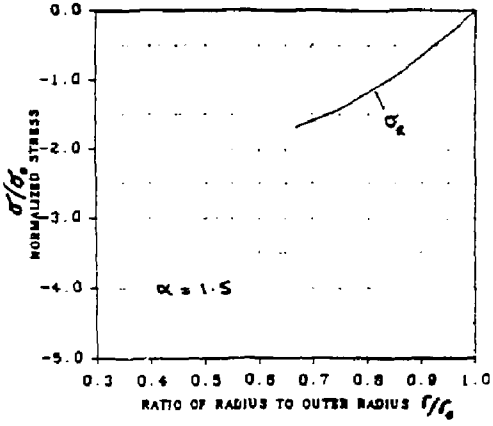

3B DISTRIBUTION OF PRINCIPAL STRESS ACROSS THE THICKNESS IN PURE BUCKING

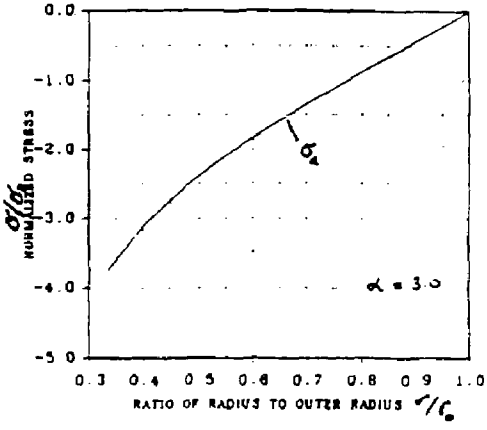

4A DISTRIBUTION OF PRINCIPAL STRESSES ACROSS THE THICKNESS IN COMBINED BUCKING AND WEDGING

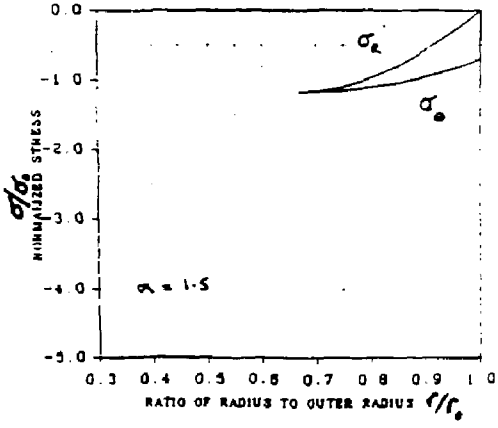

4B DISTRIBUTION OF PRINCIPAL STRESSES ACROSS THE THICKNESS IN COMBINED BUCKING AND WEDGING

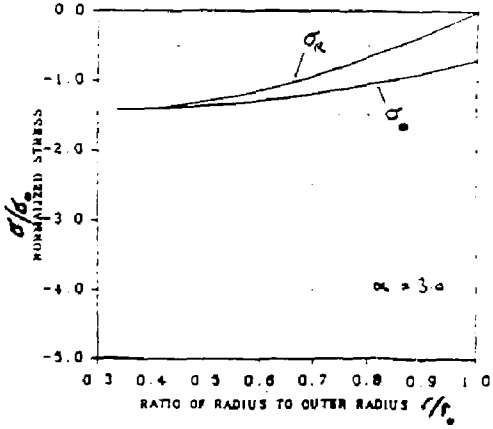

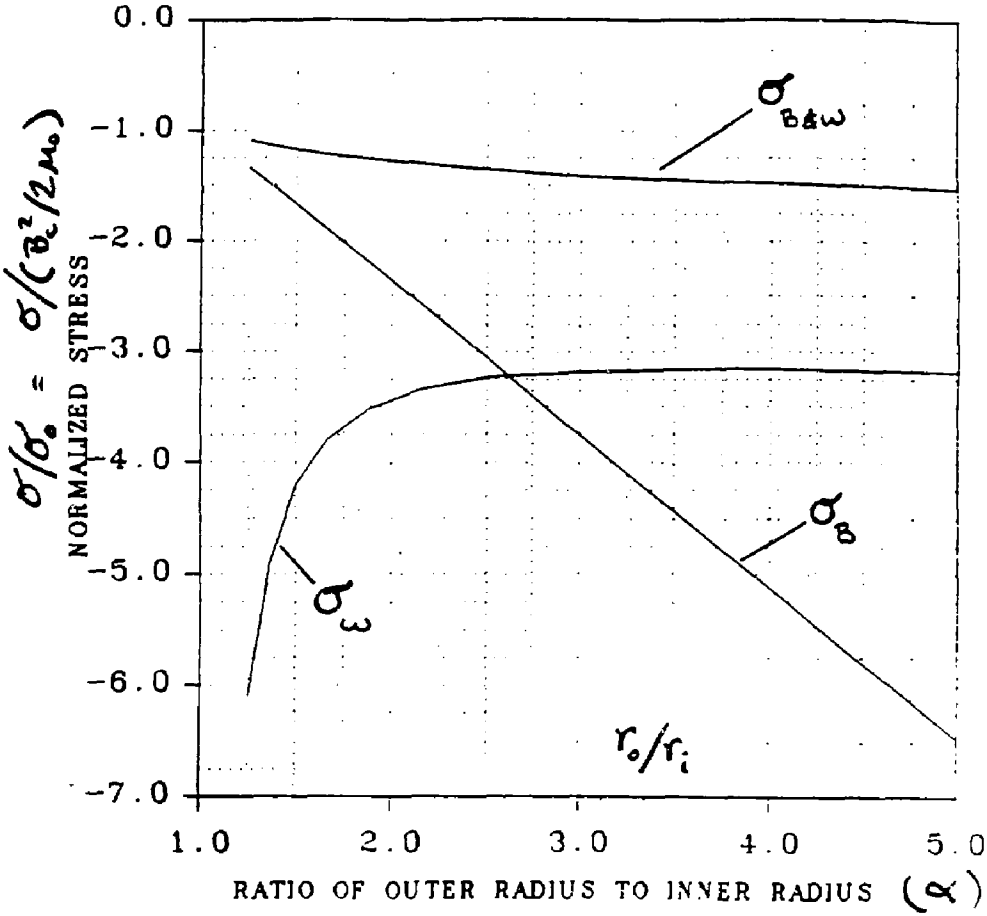

Figure 5: Normalized peak stress for pure bucking, pure wedging and combined bucking and wedging as a function of the radius ratio α, of a cylinder carrying axial current which results in a surface field, B_c.

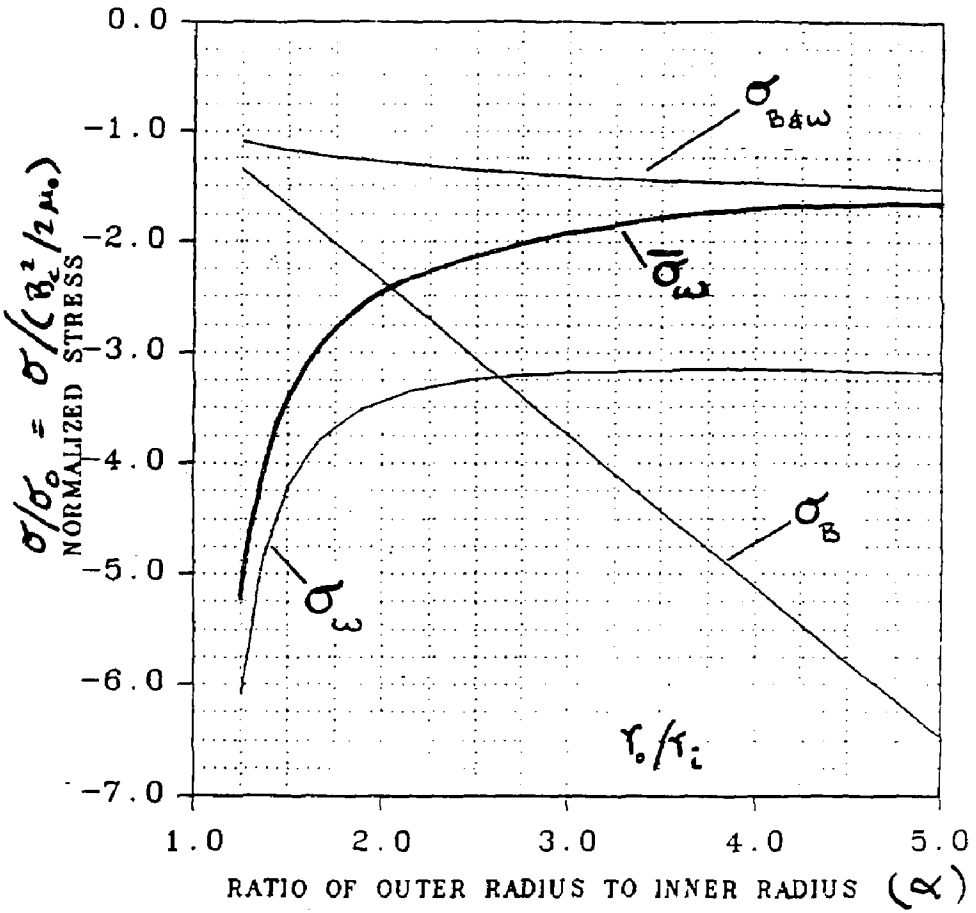

Figure 6: Normalized average wedge stress for pure wedging, compared against the peak stresses of Figure 5.

3.0 ESTIMATION OF VERTICAL STRESS

Section 2.0 considered an isolated cylindrical section in the center region, under the assumption that there was no vertical stress. The average vertical stress which would be present, or which would need to be removed by preload, can be estimated from the upward load on an ideal toroidal shell as defined in Figure. 1.

$$F_v = 2.5\ (R_o B_o)^2\ \ell n\ (\frac{r_{leg}}{r_o})\ MN$$

A toroidal magnet with R_o = 1 m, B_o = 10 T, r_{leg} = 1.5 m and r_o = 0.5 m, would have a total upward load of 275 MN.

To estimate the average vertical stress on the inner leg region, it is necessary to make an assumption of the fraction of upward load which is carried by the inner legs. This depends on the coil shape and build (as well as details of the support structure). For estimating purposes, however, one can typically assume 50% of the load on the inner region, and if that load is divided by the inner leg area, $A_c = \pi\ (r_o^2 - r_i^2)$, an approximate average vertical stress can be found. For the above example, if r_i = 0.25 m, an average vertical stress of 233 MPa would be present when 50% of the load is carried by the inner region.

4.0 IDEALIZED CALCULATIONS FOR SELECTED EXISTING AND PROPOSED TOKAMAKS

We can use Figure 5 to estimate peak stresses for bucking, wedging or combined bucking-wedging for some selected tokamaks. Table 2 gives the idealized results for the six machines in Table 1, grouped by external versus internal transformer configuration. Table 3 calibrates the estimates by comparison against values given for JET[2] and ASDEX-UPGRADE.[3] Table 3 also calibrates the estimates for average vertical tension against the same two machines. The agreement for wedging and bucking stresses, and for average vertical stress in JET are quite reasonable considering the idealization. The estimate for vertical stress, however, underestimates the separating force by an increasing amount when the magnet build is an increasing fraction of the magnet bore; this is reflected in the significant under estimation of the separating load for ASDEX-UPGRADE. A better agreement can be obtained by using the mid-line of the coil rather than the inner bore when taking the logarithm.

Table 4 estimates the idealized wedging and bucking stresses for four ignition machine cases, the first two drawn from CIT studies,[4] and the second two from high performance ohmic ignition proposals.[5,6]

We can use the two pure wedging CIT studies to illustrate some considerations for wedging versus bucking, and for external versus internal transformer placement. The two CIT

cases represent machines of comparable performance, and differ only in that one has an external transformer and one an internal transformer. For our idealized calculation of wedging or bucking stresses, the two machines differ in the radius ratio of the core, and the peak field at the winding. By locating the transformer inside the TF coil, the TF build can be greater (high radius ratio), but because the outer radius of the core is smaller, the peak field will be greater. We note from Table 4, that the wedging stresses are comparable for the two cases; the peak wedging stress is 10% higher for the internal OH case, but the average wedging stress is 15% lower. The reported vertical stresses[4] are 210 MPa for the external OH case, and 19% higher, 250 MPa, for the internal OH case. The tresca stress combining the average wedge stress with the vertical stress are within 3% for the two cases at 555 MPa for the external transformer case, and 540 MPa for the internal transformer case.

The two CIT cases use pure wedging. Figure 5 suggests that the internal transformer device, with a radius ratio of 3, will have a smaller peak stress if wedging is used rather than bucking; hence wedging was a reasonable choice. The external transformer CIT case, on the other hand, has a radius ratio of 1.6, and falls in a range where pure bucking would result in a peak stress only 48% of that which results from pure wedging. Use of bucking in this case however, would require that the TF coil be bucked against the transformer. It would also require that the coil torque be supported by a

torque structure, coil cases, or combined bucking and wedging.

Ideal combined bucking and wedging would result in reduced stresses for both of the CIT cases. The external transformer case would see only 43% of the pure wedging stresses, and the internal transformer case, 31%. As we will discuss in Section 5.0, however, achievement of the benefits of combined bucking and wedging is difficult to achieve in non-ideal machines.

The IGNITOR device proposal,[5] idealized in Table 4, depends principally on bucking, (with some wedging allowed to control out-of-plane torque in the inner leg) and is bucked against the external transformer. The IGNITOR radius ratio of 1.46, falls in the range where bucking is more attractive than wedging; in this case resulting in only 37% of the peak stress it would have, had it been wedged. Were ideal combined bucking and wedging to be assumed, the peak stresses would be further reduced to 75% of those for pure bucking.

The IGNITEX device[6] idealized in Table 4, proposes to take full advantage of combined bucking and wedging. At a radius ratio of 2.5, combined bucking and wedging results in a peak stress 44% of that which would occur were the device either purely bucked or purely wedged. IGNITEX proposes an internal transformer, and therefore can buck against a structural element rather than a transformer as in IGNITOR.

TABLE 2.0

ESTIMATED PEAK WEDGING OR BUCKING STRESS FOR TABLE 1 MACHINES

	r_i (cm)	r_o (cm)	R_o (cm)	r_{leg} (cm)	B_o (T)	B_c (T)	α	σ_{in} PEAK (MPa)	SUPPORT MODE	TRANS-FORMER LOCATION
JET	112	150	296	460	3.45	6.8	1.33	23	BUCKING	EXTERNAL
TFTR	86	140	248	420	5.2	9.2	1.63	64[a]	BUCKING	EXTERNAL
ASDEX-U	53	92	165	275	3.9	7.0	1.74	73	WEDGING	EXTERNAL
DIII	26	63	165	176	4.0	10.5	2.42	142	WEDGING	INTERNAL
JT-60	46	138	300	526	4.5	9.8	3.0	143[a]	BUCKING	INTERNAL
ALCATOR C-MOD	7.5	31	66	109	9.0	19.0	4.13	460	WEDGING	INTERNAL

NOTE (a): Peak stress at TF/Bucking post interface if the load is uniformly supported over the surface.

TABLE 3.0

CALIBRATION OF ESTIMATED STRESSES AGAINST REPORTED STRESSES

	PEAK σ_{in} ESTIMATED	PEAK σ_{in} REPORTED	RATIO	SEPARATING LOAD ESTIMATED	SEPARATING LOAD REPORTED	RATIO	AVERAGE $\sigma_{vert.}$ ESTIMATED	AVERAGE $\sigma_{vert.}$ REPORTED	RATIO
JET	23 MPa	25 MPa	0.92	292 MN	326 MN	0.9	47 MPa[a]	58 MPa[b]	0.81
ASDEX-UP	73 MPa	66 MPa	1.1	113 MN	147 MN	0.77	32 MPa[a]	42 MPa	0.76

NOTES (a): 50% of separating force assumed to be carried by inner legs over 100% of available area calculated as $\pi (r_o^2 - r_i^2)$

(b): No average tension was reported; 58 MPa is an average of reported inner and outer fiber tension in the winding pack with $\lambda \cong 0.8$; if $\lambda = 0.8$ is applied to the estimated vertical stress, the resulting 59 MPa essentially matches the reported stress.

TABLE 4.0

ESTIMATED STRESSES FOR FOUR EXAMPLES OF IGNITION DEVICES

	r_i (cm)	r_o (cm)	R_o (cm)	r_{leg} (cm)	B_o (T)	B_c (T)	α	ESTIMATED PEAK σ_{in}	SUPPORT MODE	TRANS-FORMER LOCATION
CIT 1.8 m Case External OH	74	120	180	270	11.3	17.0	1.62	449 MPa [345 MPa][a]	WEDGING	EXTERNAL
CIT 1.8 m Case Internal OH	35	104	180	270	11.3	19.5	3.0	492 MPa [290 MPa][a]	WEDGING	INTERNAL
IGNITOR -L [04/86]	45	66	109	150	12.4	20.5	1.46	277 MPa	BUCKING	EXTERNAL
IGNITEX [04/87]	40	100	150	210	20.0	30.0	2.5	479 MPa	BUCKING & WEDGING	INTERNAL

NOTES (a): Average wedging stress using Figure 6

5.0 NONIDEAL CONSIDERATIONS

We have noted in the previous sections, that ideal bucking and wedging always results in lower stresses than either bucking or wedging alone. We have also noted, that when considering pure bucking or pure wedging alone, one or the other results in lower stresses depending on the radius ratio.

When a designer chooses to employ a support option which results in lower stresses than an alternate option at the same radius ratio, it is necessary to assure that the support will actually function as expected.

For example, if bucking is chosen, and is more favorable than wedging, it is generally necessary to provide toroidal gaps to assure that the coils will buck. Without sufficiently large toroidal gaps between coils, use of an undersized bucking post for example, would result in wedging rather than bucking.

A similar situation would occur when a bucked magnet heats up relative to the bucking post. The coils would expand toroidally, close the toroidal gaps, and then the wedged assembly would expand away from the bucking post, opening up the equivalent of an assembly gap. Again sufficiently large toroidal gaps must be provided to assure that at the maximum temperature difference, the gaps do not close and transfer the support to the higher stress wedging state.

When bucking off a transformer, as opposed to a passive bucking post, further nonideal conditions for the TF are present (as well as for the transformer itself). For example, the bucking post is now "active" and will change dimensions depending on the relative temperature or stress state. As long as the design utilizes only pure bucking, expansion of the transformer will not effect the TF bucking pressure. However, if some wedging is also being used to support out-of-plane torque, expansion of the core will tend to dewedge the TF.

Unlike pure bucking or wedging, which require gaps, combined bucking and wedging, must avoid gaps if both support techniques are to act simultaneously and in the desired proportion. For example, if the coil heats relative to the passive bucking post, the coil will tend to expand away from the post, transferring more of the load to wedging, and less to bucking. On the other hand, if the magnet were to have a lower modulus than anticipated, more of the load will be taken up in bucking and less in wedging; ie., the "soft" magnet can not carry load as effectively as the "stiff" bucking post.

We can illustrate several of these nonideal effects by means of simple examples. We first estimate the effect of assembly gaps on IGNITOR in Table 5.0.

In the case of IGNITOR, pure bucking is assumed, and as discussed earlier, results in a stress only 37% of that which would have occurred had the magnet been in pure wedging. If the assembly gap in IGNITOR were to be very large, the TF magnet would never buck, and the resultant pure wedging stresses would be 2.7 times higher. Fractions of the gap that result in full wedging, add fractional wedging stresses, and relieve fractional bucking stresses. For a realistic assembly gap of 0.7 mm and zero toroidal gaps, we note that the stress will be increased by 20% above that anticipated for pure bucking.

IGNITOR has proposed to allow some wedging to take place, to support the out-of-plane torque on the inner leg. If more than an allowed distribution of toroidal gaps is present, however, the magnet will not wedge. In the case of IGNITOR, if there is no radial assembly gap, and if more than an 0.38 mm gap is present between each of 12 coils, no wedging will occur.

TABLE 5

ESTIMATED EFFECT OF RADIAL OR TANGENTIAL ASSEMBLY GAPS ON IGNITOR

RADIAL GAP[d] (mm)	PEAK STRESS MPa	TOROIDAL GAPS[e] (mm)	PEAK STRESS MPa
0	193[a]	0	193[a]
0.71	330	0.1	220
1.42	467	0.19	239
2.13	603	0.29	258
2.84	739[b]	0.38	277[c]

NOTES: [a] Ideal Bucking and Wedging
[b] Pure Wedging
[c] Pure Bucking
[d] Radial gap between TF and bucking post; toroidal gaps = 0
[e] Toroidal gaps between each of 12 coils; radial gap = 0

The effect of radial or toroidal gaps on IGNITEX, are illustrated in Table 6. In the case of IGNITEX, combined bucking and wedging is assumed, and that results in a stress 44% of that which would have occurred if either pure bucking or pure wedging had occurred. As with IGNITOR, if a sufficiently large radial gap were present, the magnet would be in pure wedging, and the stress would be 2.3 times as high. For a realistic radial assembly gap of 1.0 mm, the stress would be increased by 36%. If, on the other hand, more than an allowed amount of distributed toroidal gaps is present, the magnet will carry more load in bucking than intended. In the IGNITEX case, if more than 1.35 mm of inter-sector toroidal gap is present between the 12 sectors, the magnet would be in pure bucking, and the stress would again be 2.3 times as high. The comparable inter-turn gap (for 600 turns) would be only 0.027 mm/turn. This suggests that controlling the effective distributed toroidal turn-to-turn gaps will be important in IGNITEX. IGNITEX reports a peak combined stress of 550 MPa and a material yield of 580 MPa.

Another nonideal condition which must be accommodated in bucking and wedging, is the relative temperature of the magnet and bucking structures. Table 7 illustrates the effect on IGNITEX. The equivalent of a 1 mm radial assembly gap, and the associated 36% increase in stress, accompany a 264 K magnet temperature and a 77 K bucking post.

Finally, bucking and wedging magnets must accommodate an uncertainty in the modulus of the magnet relative to that of the bucking structure. The estimation of ideal stresses in Figure 5 assumed that the magnet and the bucking post have the same modulus. If the magnet were to have a modulus less than that of the bucking post, then proportionately more stress would be picked up by the bucking post, leading to stress conditions more like bucking. As an example, if the magnet contains 5% insulation, and if that insulation were to have a modulus 1/20 that of copper, then the magnet effective modulus would only be half that of pure copper (and half that of a typical bucking post). In the case of IGNITEX, that would raise the peak stress by 20% from 479 MPa to 576 MPa. To mitigate this condition, the designer would have to "soften" the bucking post. However, uncertainties in the modulus of the magnet, the post, and the interface insulation, will always lead to an unpredictable balance of bucking and wedging, warning the designer not to count on the theoretical optimum balance.

Nonideal conditions make it difficult to achieve the maximum benefits of bucking and wedging. Provided that the design is sufficiently robust to operate off the optimum balance, however, partial wedging, or partial bucking can be considered to relieve some fraction of the pure bucking or pure wedging stresses. As an example, a wedged design might utilize a bucking post which engaged only after the nominal operating field closed a radial assembly gap. Up-grade fields beyond the nominal might then be feasible.

TABLE 6

EFFECT OF RADIAL OR TOROIDAL ASSEMBLY GAPS ON IGNITEX

RADIAL GAP[d] (mm)	PEAK STRESS (MPa)	TOROIDAL GAPS[e] (mm)	PEAK STRESS (MPa)
0	479[a]	0	479[a]
1.0	652	0.34	629
2.0	825	0.68	779
3.0	997	1.01	850
4.0	1,170[b]	1.35	1,080[c]

NOTES:
[a] Ideal bucking and wedging
[b] Pure wedging
[c] Pure bucking
[d] Radial gap between TF and bucking post; toroidal gaps = 0
[e] Toroidal gaps between each of 12 sectors; radial gap = 0

TABLE 7

IMPACT OF MAGNET TEMPERATURE ON BUCKING AND WEDGING IN IGNITEX (BUCKING POST ASSUMED TO REMAIN AT 77 K)

TEMPERATURE (°K)	EQUIVALENT GAP (mm)	PEAK STRESS (MPa)
77	0	479
264	1	652
388	2	825

6.0 TYPICAL TOKAMAK UNCERTAINTIES

6.1 Rotation of the JET Transformer

JET has recently removed their central transformer for modification, and in doing so, caught an incipient problem that would have eventually resulted in major damage. The out-of-plane torque on the TF coils is transferred to the torque tube, which is in turn attached to the upper and lower portions of the torque shell. Apparently the TF coil torque was transferred through the torque tube to the transformer coils, rotating those coils, and shearing the insulating keys. The coils then gradually rotated through a large angle and were close to breaking the leads. A ruptured lead would have resulted in major arc damage.

6.2 TFTR Bucking Structure

The TFTR TF coils buck against a structure which contains the central transformer coils, but the bucking load is taken on rings rather than on the coils. The out-of-plane torque on the inner portion of the magnet is supported by keying the coil cases into the bucking structure; the torque on the outer section is taken by wedging the coils with shear panels. During the early analysis of TFTR, the designers had considerable difficulty assuring themselves that the outer shear panels would wedge properly and take the anticipated share of the load. The bucking structure was too stiff relative to the coil, and took too much of the load. After several different approaches were considered, it was decided to

substitute titanium for steel in the bucking structure to "soften" that structure.[7]

6.3 Load Sharing in the JT-60 TF Coil Cases and Windings

Measurements on the JT-60 coil cases during tokamak operation indicated that the coil case strains were half those predicted by finite element analysis. This is believed to be due to an unexpected gap between the TF coils and the case, and resulted in the coils carrying more than the theoretical share of the load. Subsequent analysis has convinced the designers however, that the increased coil stress will not be of concern.[8]

7.0 RECOMMENDATIONS FOR CIT

7.1 CIT designs which use an external transformer, should use pure wedging despite the reduced TF stresses which would result if the TF coil were bucked against the transformer. The 215 MPa interface pressure on the transformer which would be present in the CIT example, were pure bucking used, is essentially an order of magnitude larger than that estimated for JET (23 MPa). We do not believe it is prudent to subject the transformer to these external pressures, and at the same time to assure that the proper sliding of the interfaces can take place during twist and relative axial expansions.

7.2 CIT designs which use an internal transformer typically fall in a radius ratio where wedging is more attractive than bucking, and we recommend pure wedging for this case.

7.3 CIT designs which allow realistic assembly gaps, temperature differences, and modulus uncertainty, greatly reduce the attractiveness of combined bucking and wedging. We recommend that CIT designs not utilize combined bucking and wedging in any primary support strategy.

REFERENCES

1. This approach parallels similar ideal comparisons made by P. Bonanos and J. Bialek in PPPL internal memos in the summer of 1984.

2. The JET Project, Scientific and Technical Developments, EUR 5791e, 1977.

3. ASDEX-UPGRADE, ASDEX Upgrade Project Proposal, Phase II, IPP 1/217, May 1983.

4. L. Bromberg, ERB Meeting, April 9-10, 1987.

5. IGNITOR Project Feasibility Study, ENEA Contract 25878, Status Report, March 31, 1986.

6. IGNITEX, Basic Design Report for the Fusion Ignition Experiment, March 1987.

7. TFTR TF Coil Support Restraint Structure, L. Blumenau, J. Citrolo, J. Bialek, G. Cargulia, CH1441-5/79/0000-0113, IEEE 1979.

8. JT-60 Power Testas from Mechanical and Thermal Viewpoints of Tokamak Machine, H. Takatsu et al., CH2251-7/86/0000-0813, IEEE 1986.

APPENDIX A

A.1 Formulas for pure wedging

$$\rho \equiv \frac{r_i}{r_o}$$

$$r_* \equiv \frac{r}{r_o}$$

$$\alpha \equiv \frac{1}{\rho} = \frac{r_o}{r_i}$$

$$\sigma_r^* \equiv \frac{\sigma_r}{\frac{B_o^2}{2\mu_o}} = \frac{1}{2(1-\rho^2)^2}\left\{(3+\nu)(r_*^2-\rho^2)+4(1+\nu)\rho^2 \ln\frac{\rho}{r_*}\right.$$

$$\left. + \left[-(3+\nu)-4(1+\nu)\left(\frac{\rho^2}{1-\rho^2}\right)\ln\rho\right]\left[1-\left(\frac{\rho}{r_*}\right)^2\right]\right\}$$

$$\sigma_\theta^* \equiv \frac{\sigma_\theta}{\frac{B_o^2}{2\mu_o}} = \frac{1}{2(1-\rho^2)^2}\left\{(1+3\nu)r_*^2+(1-5\nu)\rho^2\right.$$

$$+\left[1+\left(\frac{\rho}{r_*}\right)^2\right]\left[-(3+\nu)-4(1+\nu)\frac{\rho^2}{1-\rho^2}\ln\rho\right]$$

$$\left. + 4(1+\nu)\rho^2 \ln\frac{\rho}{r_*}\right\}$$

$$\sigma^*_{\theta\,peak} \equiv \frac{\sigma_{\theta\,peak}}{\frac{B_o^2}{2\mu_o}} = \frac{1}{(1-\rho^2)^2}\left[(1-\nu)\rho^2 - (3+\nu) - 4(1+\nu)\frac{\rho^2}{1-\rho^2}\ln\rho\right]$$

Peak value is evaluated at $r = r_i$ or $r_* = \rho$.

$$\sigma^*_{\theta\,ave} \equiv \frac{\sigma_{\theta\,ave}}{\frac{B_o^2}{2\mu_o}} = \frac{4}{3}\cdot\frac{1}{(1-\rho^2)^2}(2\rho+1)(\rho-1)$$

$$u^*_{r|r=r_i} \equiv \frac{u_{r|r=r_i}}{r_i}$$

$$= \left[\frac{\frac{B_o^2}{2\mu_o}}{\frac{E}{1-\nu}}\right]\frac{1}{(1-\rho^2)^2}\left\{\rho^2 - \frac{1}{1-\nu}\left[(3+\nu) + 4(1+\nu)\left(\frac{\rho^2}{1-\rho^2}\right)\ln\rho\right]\right\}$$

A.2 Formulas for pure bucking

$$\sigma_r^* \equiv \frac{\sigma_r}{\frac{B_z^2}{2\mu_0}} = -\frac{4}{3}\frac{1}{(1-\rho^2)^2}\left[\frac{1}{r_*} - 1\right]\left[1 + r_* + r_*^2 - 3\rho^2\right]$$

$$\sigma_{r\,peak}^* = -\frac{4}{3}\frac{1}{\rho(1+\rho)^2}(1+2\rho)$$

A.3 Formulas for Combined bucking and Wedging

$$\sigma_r^* \equiv \frac{\sigma_r}{\frac{B_o^2}{2\mu_o}} = \frac{1}{2(1-\rho^2)^2}\left[(3+\nu)(r_*^2-1)\right.$$

$$\left. - 4(1+\nu)\rho^2 \ln r_* + \rho^4(1-\nu)\left(\frac{1}{r_*^2}-1\right)\right]$$

$$\sigma_\theta^* \equiv \frac{\sigma_\theta}{\frac{B_o^2}{2\mu_o}} = \frac{1}{2(1-\rho^2)^2}\left[(1+3\nu)\, r_*^2\right.$$

$$- 4(1+\nu)\rho^2 \ln r_* - (3+\nu)$$

$$\left. - \rho^4(1-\nu)\left(1+\frac{1}{r_*^2}\right) + 4\rho^2(1-\nu)\right]$$

$$\sigma_{\theta\,peak}^* = \frac{\sigma_{\theta\,peak}}{\frac{B_o^2}{2\mu_o}} = \frac{1}{2(1-\rho^2)^2}\left[4\rho^2 - 4(1+\nu)\rho^2 \ln\rho\right.$$

$$\left. - (3+\nu) - (1-\nu)\rho^4\right]$$